Materials Transactions, Vol. 46, No. 6 (2005) pp. 1301 to 1305

Evaluation of Grain Boundary Effect on Strength of Fe–C Low Alloy Martensitic Steels by Nanoindentation Technique

Jinxu Li[1], Takahito Ohmura[2] and Kaneaki Tsuzaki[2]

[1]*Department of Materials Physics, University of Science and Technology Beijing, 100083, P. R. China*
[2]*Steel Research Center, National Institute for Materials Science, Tsukuba 305-0047, Japan*

The grain boundary effect on the strength was evaluated through nanoindentation technique for Fe–0.4C–Cr–Mo steels that were produced by the ausform-tempered (AF) and conventional quench-tempered (QT) processes. A semiquantitative Hall–Petch plot was made to determine the locking parameter k for the two alloys using nanohardness, micro-Vickers hardness, and grain size. The k value for the QT sample is significantly larger than that for the AF sample and is attributed to the film-like carbides on the grain boundaries of the QT sample. The lower k value of the AF sample is one of the factors for the improved delayed fracture property in the AF compared to that of the QT sample.

(Received January 28, 2005; Accepted April 19, 2005; Published June 15, 2005)

Keywords: *nanoindentation, iron-carbon low alloy steel, tempered martensite, Hall–Petch plot, grain boundary, locking parameter, carbide*

1. Introduction

Fe–C based martensitic steels are considered to be among the important high-strength materials that are utilized for automobile parts and construction components. To improve the performance and reliability of high-strength steels, it is important to reveal the strengthening mechanisms on the statistic strength and the fracture strength such as fatigue and delayed fracture. The strength of martensitic steels has been shown to be closely related to microstructures such as grain size, dislocation density, solid solution of carbon, and its rearrangement.[1–5] However, the relationship between high strength and microstructure is still not clear because martensitic steels have a very fine and complex structure in a sub-micron scale.[6–9] Recent progress in nanoindentation technique has made it possible to evaluate the strength in nano scale. Ohmura *et al.*[10–13] performed the nanoindentation measurement within a matrix of martensite and evaluated the strengthening factors of the matrix and the grain boundary separately. This study indicated that there is a significant grain boundary effect on the macroscopic strength. The grain boundary effect depends on the characteristics of the boundary including a state of carbide precipitation, which also affects the fracture strength strongly because crack initiation and propagation occur frequently on a grain boundary. Therefore, the evaluation of the grain boundary effect is a key subject for understanding the strengthening mechanisms of not only the statistic strength but also the fracture behavior. In the present paper, two martensitic steels that were produced by ausformed-tempered (AF) and conventional quench-tempered (QT) processes with the same chemical composition of 0.4%C–Cr–Mo were used. The critical diffusible hydrogen content, below which the specimen does not fracture at a constant applied load within a certain time, is 0.13 ppm for the QT sample and 0.53 ppm for the AF. This means that the AF sample has a much higher performance on the delayed fracture than that of the QT sample, but has almost the same tensile strength of 1600 MPa class.[14] The objective of this work is to evaluate the grain boundary effect on the statistic macro-strength for the two martensitic steels with different microstructures and to consider their relation to the hydrogen-induced delayed fracture property.

2. Experimental

A commercial medium-carbon low alloy steel was used. The chemical composition of the steel is listed in Table 1. Two procedures were employed to obtain the different microstructures. Figure 1 represents a schematic of the thermomechanical processes. In the (a) ausform-tempered (AF) process, a bar with a diameter of 7.75 mm was austenitized at 1323 K for 1.2 ks, deformed by bar rolling with a 50% reduction in the cross-section area at 1063–1093 K, water quenched, and subsequently tempered at 813 K for 10 s with induction heating. In the (b) conventional quench-tempered (QT) process, a specimen was austenitized at 1153 K for 0.9 ks, oil-quenched, and subsequently tempered at 673 K for 1.8 ks in a salt bath furnace. The details of the processes are shown elsewhere.[14] The tensile strength of the AF and QT specimens was 1579 and 1586 MPa, and the Vickers hardness was 470 and 462, respectively. All the specimen surfaces were mechanically polished and electropolished in a solution of 8% perchloric, 10% butylcellosolve, 60% ethanol and 22% water at 273 K under the potential of 40 volts. The roughness of the electrically polished specimen surfaces was estimated to be about 10 nm in RMS on atomic force microscope images for both steels.

Nanoindentation experiments were performed using a Hysitron TriboIndenter® which provides both nanomechan-

Table 1 Chemical composition of the sample (mass%).

C	Si	Mn	P	S	Cr	Mo	Al	Ti	O	N	Fe
0.40	0.25	0.79	0.016	0.017	1.12	0.17	0.020	0.002	0.0008	0.0037	Bal.

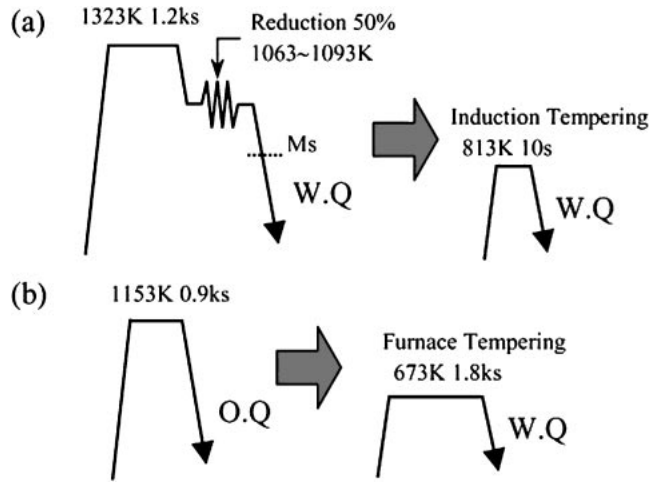

Fig. 1 Schematic of the thermomechanical process of (a) AF and (b) QT samples.

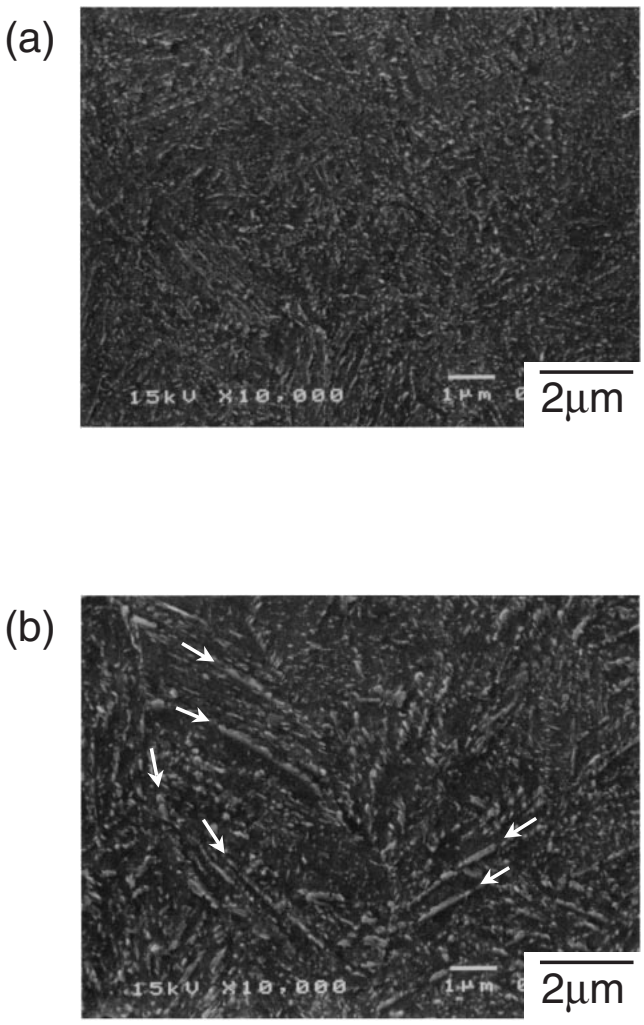

Fig. 2 SEM micrographs showing carbide structures of (a) AF and (b) QT samples.

ical testing and *in situ* scanning prove microscope (SPM) imaging capability. A peak load of 500 μN was used. A three-sided pyramid with an apex angle of 115°, which is called the Berkovich indenter, was employed, and the tip truncation was calibrated using a reference specimen of fused silica. Analyses for the tip calibration and the calculation of nanohardness were conducted using the method outlined by Oliver and Pharr.[15] Electron backscatter diffraction (EBSD) analysis was carried out to measure the grain size of the specimens using a Carl-Zeiss LEO-1550 Schottky Field Emission SEM fitted with a TexSEM Lab. The specimen surface after indentation was observed with the SPM capability of the Triboindenter. Conventional micro-Vickers hardness tests were carried out at an applied load of 9.8 N as a macroscopic strength measurement using a MVK-H2 micro-Vickers hardness tester.

3. Results

3.1 Microstructure

Figure 2 represents the SEM micrographs of the carbide structure of the (a) AF sample and the (b) QT sample. The AF sample has fine uniformly distributed carbide particles and does not show any visible grain boundaries on the image. In the QT sample, coarse film-like carbides precipitate on the prior γ grain boundary or block boundary, as indicated by the arrows. Since a volume fraction of carbide depends only on the carbon content, and the size of the carbide is larger for the QT sample than that for the AF sample, an average spacing between carbide particles in the AF sample is much smaller than that in the QT sample. These results are consistent with the ones in the previous paper.[14]

Figure 3 shows SPM images of the (a) AF and the (b) QT samples taken after the nanoindentation test. Triangle indent marks appear on the images of both samples. The size of the indent marks is estimated to be about 300 nm. The images also show film-like carbides on the boundaries of the QT sample and a homogeneous carbide distribution in the AF sample.

Another important factor of the microstructure is the grain size. The previous studies[6–9] on the morphology of the lath martensite showed the presence of four structural units. The largest one is the prior austenite grain, which consists of packets, the packet is composed of blocks with the same habit plane, and the block is sub-divided into a lath structure. Only the lath boundary has a low-angle among them; therefore, the block structure can become analogous to a grain if the high-angle boundary is assumed to be a grain boundary. Figure 4 shows the grain distribution maps that were obtained by the EBSD analysis for the two samples. The solid lines represent misorientation angles that are larger than 10°. According to the variants model in the K–S relationship for the lath martensite,[16] the minimum misorientation angle is 10.53° among the four possible block boundaries with the same habit plane. Additionally, the accuracy of the orientation measurement in the EBSD analysis is within 0.2°. Therefore, the grain represented in Fig. 4 could be regarded as a block structure. The average grain size was determined to be 1.8 and 3.9 μm for the AF and QT, respectively.

3.2 Hardness test

Typical load-displacement curves for the AF and QT samples are shown in Fig. 5. The conducted peak load was

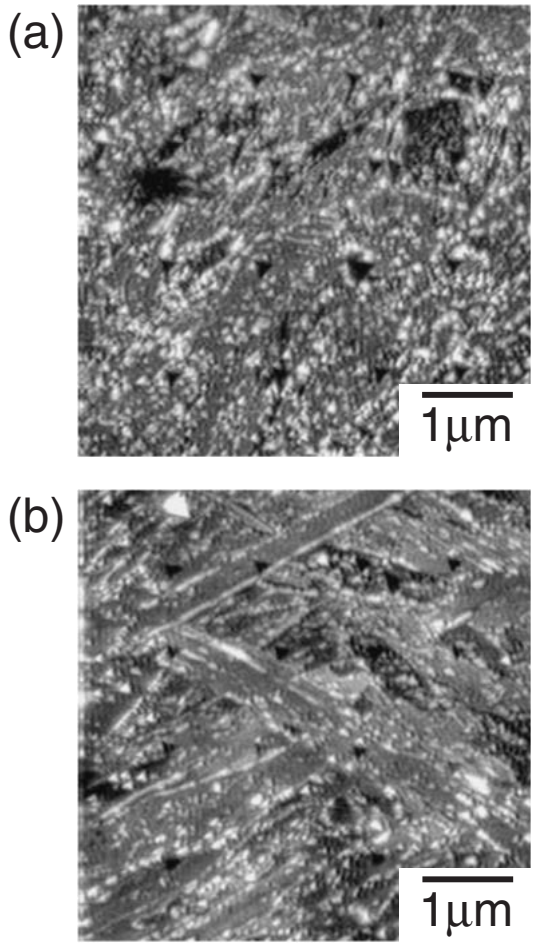

Fig. 3 SPM images representing indent marks on the specimen surface after indentation of (a) AF and (b) QT samples.

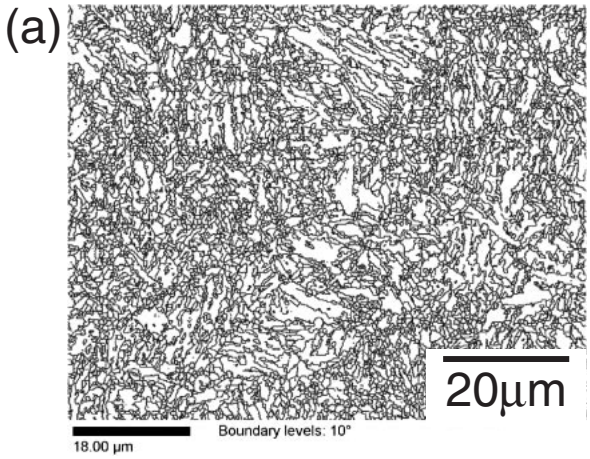

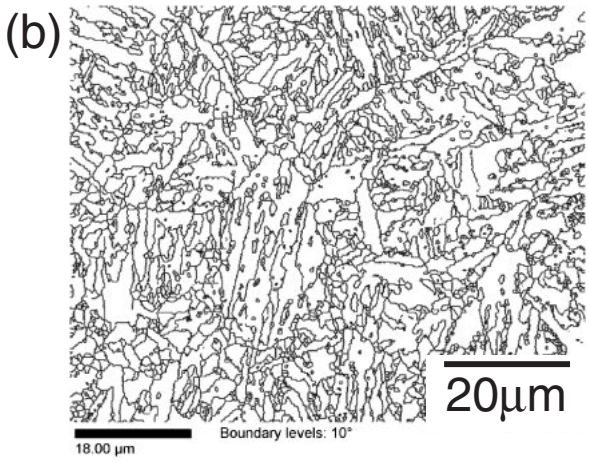

Fig. 4 Grain distribution maps of (a) AF and (b) QT samples obtained by the EBSD analysis.

500 μN, and the corresponding penetration depth ranged around 40 nm. The average nanohardness calculated from 120 random measurement points for the AF and QT samples were 8.47 ± 1.76 GPa and 7.98 ± 1.95 GPa, respectively. The average for the AF sample is slightly larger than that for QT sample. The data is scattered significantly around the average value, which may be due to the distribution of the carbide particles. The Micro-Vickers hardness for the AF and QT samples was 470 ± 7.15 and 462 ± 7.04, respectively. These values are consistent with the tensile strength of the samples.

4. Discussion

The indentation-induced plastic zone size should be compared to the grain size to evaluate the matrix strength that is separated from the grain boundary effect. As described above, the typical penetration depth is about 40 nm, and the size of the indent mark is around 300 nm. Using the hemispherical approximation of a plastic zone size beneath the indenter,[17] the diameter of the plastic zone is about 360 nm which is about nine-times larger than the penetration depth. The estimated plastic zone size is much smaller than the average grain size of 1.8 or 3.9 μm described in Fig. 4; hence the measured nanohardness is dominated by the matrix

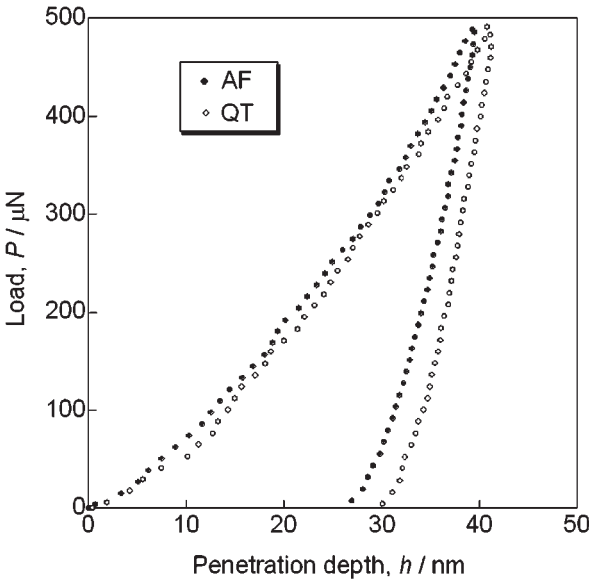

Fig. 5 Typical load-displacement curves for AF and QT samples.

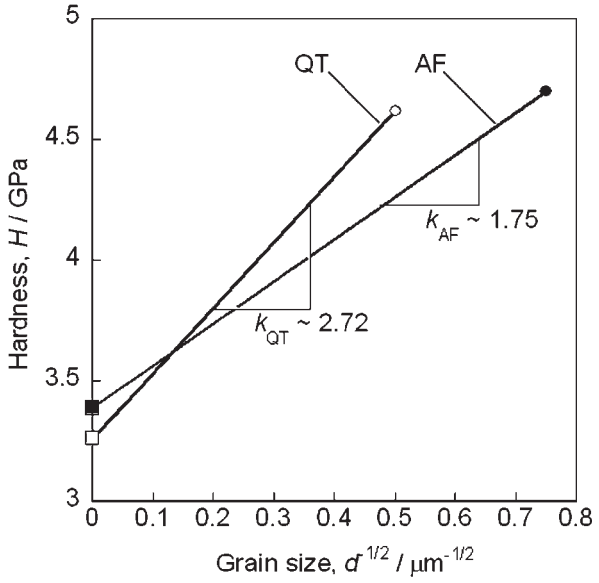

Fig. 6 Semiquantitative Hall–Petch plot of AF and QT samples.

strength of the martensite with little contribution from the high-angle boundaries. While it is possible that a grain boundary may exist just beneath the indenter or within the plastic zone in some cases, the number of the boundaries associated with the plastic zone could only be a few at the most, and the effect of the grain boundary is considered to be relatively small.[12)]

We assume that the statistic macro-strength of the martensite consists of the two factors that are associated with the matrix and the grain boundary and express it as:

$$\sigma = \sigma_0 + kd^{-n}, \tag{1}$$

where σ is the flow stress, σ_0 is the overall resistance of the crystal lattice to the dislocation movement, k is the locking parameter, d is the grain diameter and n is the positive constant. The grain boundary effect can be considered on a Hall–Petch plot by using the hardness associated with the flow stress of the tensile test. Figure 6 shows the semi-quantitative Hall–Petch plot of the AF and QT samples. The solid and open marks refer to the AF and QT sample, respectively. To plot the nanohardness Hn (squares) with the Vickers hardness Hv on the same axis, Hn is converted to Hv using an empirical equation of $Hn = 2.5Hv$ for bcc single crystals with a 500 μN peak load condition that was shown in previous papers.[10,12)] Additionally, nanohardness can be regarded as σ_0 plotted on the y axis because σ_0 indicates a stress for a sample with a grain size of infinity and corresponds to the matrix strength without any contribution of the grain boundary. On the other hand, the conventional micro-Vickers hardness (circles) for the two samples can be plotted using the grain size data obtained by the EBSD analysis described in Fig. 4. Then the slope of each sample can be drawn, and the locking parameter k of the AF and QT can be obtained as 1.8 and 2.7 $MNm^{-3/2}$, respectively, with a remarkable difference of about 50%.

As generally understood, the locking parameter k is associated with the resistance to the deformation transfer from a grain to an adjacent grain at a grain boundary. To interpret the difference in k for the AF and QT samples, the deformation behavior is considered based on the dislocation pile-up model. As dislocations pile up on a slip plane against a grain boundary, the stress is transferred to the adjacent grain. The shear stress τ at the dislocation source in the adjacent grain is expressed as

$$\tau = \alpha\tau_s(L/r)^{1/2}, \tag{2}$$

where α is the orientation-dependent factor close to unity, τ_s is the average resolved shear stress on the slip plane, L is the distance along the slip plane between the head of the pile-up and the hindward dislocation source, which is directly proportional to the number of pile-up dislocations, and r is the distance from the head of the pile-up to the forward dislocation source in the adjacent grain.[18)] When film-like carbides exist at the grain boundary, they enlarge the distance r and shorten the distance L by an amount that is equal to the thickness of the carbide, hence; the shear stress τ in the adjacent grain decreases. Therefore, the locking parameter k of the AF sample is smaller than that of the QT sample.

For the delayed fracture properties of the two samples, the following consideration can be drawn from the grain boundary effect. Since the carbide is much harder than the ferrite, the grain boundary with the film-like carbide is a strong obstacle for the dislocation glide motion. Therefore, the stress concentration at the grain boundary is much higher in the QT sample than that in the AF sample. Additionally, the higher stress concentration may lead to a higher strain concentration because the matrix strength is almost the same or slightly lower for the QT sample. In any criterion of stress or strain, the crack initiation and propagation along the grain boundary is inhibited in the AF sample because of the low stress/strain concentration with the low k value. A tensile stress region in a specimen is attractive for diffusible hydrogen in a specimen especially for the hydrogen-induced fracture behavior; hence, the lower stress concentration leads to a lower hydrogen concentration. Accordingly, the higher delayed fracture resistance in the AF sample is partly attributed to its low k value.

5. Summary

The grain boundary effect on the statistic strength was evaluated through nanoindentation technique for the Fe–0.4C–Cr–Mo steels that were produced by the ausform-tempered (AF) and the conventional quench-tempered (QT) processes. The nanohardness associated with the matrix strength is almost the same for the two alloys.

The Micro-Vickers hardness and the tensile strength are also pretty much the same for the alloys. On the other hand, the average block size, which is analogous to the grain size of the QT sample, is twice as large as that of the AF sample. Using these mechanical and microstructural characteristics, the semiquantitative Hall–Petch plot was made for each alloy, and the locking parameter k was determined to be about 50% smaller for the AF sample than that of the QT sample. The difference in k for the two alloys are attributed to the different carbide structures on the grain boundaries, *i.e.* the QT sample shows film-like carbides on the grain boundaries while the AF sample consists of fine carbide

particles with a homogeneous distribution and does not contain any film-like carbides. Since the grain boundary with a film-like carbide is a major stress concentration site, the low k value of the AF sample is considered to be one of factors for the higher resistance to the hydrogen-induced delayed fracture property.

Acknowledgement

The authors would like to express their gratitude to the Japan Society for the Promotion of Science for providing a JSPS Postdoctoral Fellowship [ID: PB 01734].

REFERENCES

1) W. C. Leslie and R. J. Sober: Trans. ASM **60** (1967) 459–484.
2) L.-A. Norstrom: Scand. J. Metall. **5** (1976) 159–165.
3) F. B. Pickering: *Hardenability Concepts with Applications to Steel*, (AIME, Warrendale, PA, USA, 1978) pp. 179–220.
4) G. Krauss: *Hardenability Concepts with Applications to Steel*, (AIME, Warrendale, PA, USA, 1978) pp. 229–248.
5) G. Krauss: Mater. Sci. Eng. A **273–275** (1999) 40–57.
6) A. R. Marder and G. Krauss: Trans. ASM **60** (1967) 651–660.
7) J. M. Marder and A. R. Marder: Trans. ASM **62** (1969) 1–10.
8) A. R. Marder and G. Krauss: Trans. ASM **62** (1969) 957–963.
9) T. Maki, K. Tsuzaki and I. Tamura: Trans ISIJ **20** (1980) 207–214.
10) T. Ohmura, K. Tsuzaki and S. Matsuoka: Scr. Mater. **45** (2001) 889–894.
11) T. Ohmura, K. Tsuzaki and S. Matsuoka: Philos. Mag. A **82** (2002) 1903–1910.
12) T. Ohmura, T. Hara and K. Tsuzaki: J. Mater. Res. **18** (2003) 1465–1470.
13) T. Ohmura, T. Hara and K. Tsuzaki: Scr. Mater. **49** (2003) 1157–1162.
14) S. Terasaki, S. Sakashita, S. Takagi, Y. Kimura and K. Tsuzaki: Workshop on New Generation Steel, (The Chinese Society for Metals Beijing, China, 2001) pp. 239–244.
15) W. C. Oliver and G. M. Pharr: J. Mater. Res. **7** (1992) 1564–1583.
16) G. Kurdjumov and G. Sachs: Zeits. Phys. **64** (1930) 325–343.
17) M. Itokazu and Y. Murakami: Trans. Jpn. Soc. Mech. Eng. A **59** (1993) 2560–2568.
18) J. D. Eshelby, F. C. Frank and F. R. N. Nabaro: Philos. Mag. **42** (1951) 351.